Environmental Science Nano

PAPER

Cite this: *Environ. Sci.: Nano*, 2018, 5, 2699

Effects of molecular weight fractionated humic acid on the transport and retention of quantum dots in porous media†

Jiangli Yang,‡[a] Piao Xu,‡[a] Liang Hu,‡[b] Guangming Zeng,*[a] Anwei Chen,*[c] Kai He,[a] Zhenzhen Huang,[a] Huan Yi,[a] Lei Qin[a] and Jia Wan[a]

Although humic acid (HA) plays an important role in the fate and transport of nanoparticles in subsurface environments, the roles of specific fractions of HA in the transport of nanoparticles are still not well understood. In this study, quantum dots (QDs) with carboxyl and amino modifications (QD–COOH and QD–NH_2) were used as typical nanoparticles to understand the effects of molecular weight (MW) fractionated humic acid (M_f-HA) on the transport and retention behaviour of nanoparticles. Transport experiments on QDs were performed both in the absence and presence of pristine- and M_f-HA in both NaCl and $CaCl_2$ solutions at pH 7.0. The M_f-HA had distinct effects on the transport and retention behavior of QDs, which were highly dependent on the MW of the M_f-HA. In addition, the surface coating of the QDs and cation types also showed significant effects on the transport behavior of QDs. In NaCl solution, the transport of QD–NH_2 was dramatically enhanced in the presence of pristine- and M_f-HA, and the high MW M_f-HA (>100 kDa and 30–100 kDa) could enhance the mobility of the QDs more significantly than the low MW M_f-HA (10–30 kDa, 3–10 kDa, and <3 kDa). QD–COOH was readily mobile in the sand column and the recovery of injected QD–COOH was significantly higher in the presence of pristine- and M_f-HA. In $CaCl_2$ solution, the transport of QD–COOH was enhanced in the presence of pristine- and M_f-HA, and the enhancement significantly correlated with the MW of the M_f-HA. However, the transport behavior of QD–NH_2 was not altered by the pristine- and M_f-HA. Overall, these findings can improve our understanding of the effects of M_f-HA on the transport and retention of nanoparticles in subsurface environments, and suggest that the HA, surface coating and cation types are likely key factors which govern the stability and mobility of nanoparticles in the natural environment.

Received 19th May 2018,
Accepted 28th September 2018

DOI: 10.1039/c8en00535d

rsc.li/es-nano

Environmental significance

Humic acid (HA) is ubiquitous in the environment and plays an important role in the transport and fate of nanoparticles. As HA is a heterogeneous complex of organic compounds, it is still not well understood how a specific HA component influences the transport and fate of nanoparticles. In this study, we investigate how the molecular weight of HA influences the transport and retention of quantum dots (QDs) in porous media. In addition, the impacts of surface coating and cation types are also investigated. The results show that different MW fractions of HA played significantly different roles in the transport of QDs. The high MW HA fractions enhanced the transport of QDs more significantly than the low MW HA fractions. This finding reveals that different fractions of HA from the natural environment will exhibit many distinguishing effects on the transport and fate of nanoparticles. In short, this study extended our understanding on the effect of the physicochemical heterogeneity of HA on the transport of nanoparticles, as well as the influence of multiple coupled factors on the transport of nanoparticles.

[a] *College of Environmental Science and Engineering, Hunan University, and Key Laboratory of Environmental Biology and Pollution Control (Hunan University), Ministry of Education, Changsha, Hunan 410082, P.R. China. E-mail: zgming@hnu.edu.cn; Fax: +86 731 88823701; Tel: +86 731 88822829*

[b] *School of Minerals Processing and Bioengineering, Central South University, Changsha, 410083, P.R. China*

[c] *College of Resources and Environment, Hunan Agricultural University, Changsha, Hunan, 410128, PR China. E-mail: A.Chen@hunau.edu.cn*

† Electronic supplementary information (ESI) available. See DOI: 10.1039/c8en00535d

‡ These authors contributed equally to this article.

1. Introduction

Over the past decade, engineered nanoparticles (ENPs) have been increasingly applied to a variety of commercial products due to their unique physical–chemical properties.[1,2] Extensive studies have investigated the applications of ENPs in the removal of organic and inorganic contaminants.[3–10] During production, application and disposal processes, ENPs could be inevitably released into the surrounding environment.

Once they enter the environment, ENPs could undergo complicated physical and chemical transformations, including aggregation, adsorption, deposition, dissolution, and release of toxic ions or reaction with other materials/contaminants existing in the environment.[11–13] Furthermore, the ENPs will act as a new type of pollutant and pose a threat to the natural environment and human health. Thus, it is important and urgent to understand the fate and transport of ENPs in the environment and evaluate the potential impact of ENPs on the environment and human health.

Numerous studies have been conducted to investigate the transport and retention of ENPs in porous media through columns packed with quartz sand or glass beads.[14–27] Factors such as ENP properties[23,24] (*e.g.*, particle size, shape, preparation methods, concentration, and surface chemistry properties), environmental conditions[14,17,19,25–27] (*e.g.*, solution ionic strength and pH, cation type and valence, natural organic matter, surfactant, bacteria and biofilm), and collector physicochemical heterogeneities[15,19,20] (*e.g.*, grain size, type, surface coating, and roughness) have been systematically evaluated for their influence on the transport and retention behavior of ENPs in a sand column. For example, Torkzaban *et al.*[15] observed a negligible deposition of quantum dots in ultrapure sand, but the retention was more pronounced in columns packed with goethite-coated sand. Kasel *et al.*[24] reported that the depth-dependent retention coefficient and the maximum solid-phase concentration of multi-walled carbon nanotubes increased with the decrease of grain size. In general, the solution chemical properties such as ionic strength and pH, influence the stability and mobility of nanoparticles by changing the surface charge or screening the interaction of the electrical double layer (EDL).[28,29] The stability of nanoparticles depends more on the ionic composition in suspension than the ionic strength.[15] In addition, a recent study has found that the co-presence of suspended bacteria could enhance the transport of titanium dioxide nanoparticles through electrosteric and electrostatic effects.[27] However, the above discussed studies only considered the individual influence of each environmental factor on the ENP transport. In order to understand the fate and potential influences of ENPs in the environment, we must investigate how the transport behaviours of ENPs are affected by the multiple environmental factors present in the natural environment.

Humic acid (HA), which represents an active and important part of NOM, is ubiquitous in soil and groundwater environments.[30] Previous studies have demonstrated that HA plays an important role in the fate and transport of ENPs.[25,29,31–34] Adsorption of HA on the surface of ENPs would alter the physicochemical properties of the ENPs, and consequently affect the mobility and stability of the ENPs in the aquatic environment.[25,31] For example, Quevedo *et al.*[16] observed that the adsorbed HA on the Al_2O_3 surface caused charge reversal of the collector and then reduced the deposition rates of the QDs. Jiang *et al.*[35] found that HA could enhance the mobility of zinc oxide nanoparticles, even at a concentration of HA of as low as 1 mg L^{-1} of total organic carbon. Moreover, Chen *et al.*[36] reported that the aggregation of fullerene nanoparticles was enhanced when HA and Ca^{2+} existed in the suspensions, which was due to the bridging between HA, Ca^{2+} and the NPs. However, as HA consists of various mixtures of organic compounds with different sizes of molecules,[37–39] bulk HA characteristics may be insufficient representations of the specific HA components interacting with nanoparticles. Recent research[40] revealed that humic acid in the molecular weight range of 0.5–2 kDa had preferential adsorption ability on carbon nanotubes, while the smallest characterized fraction (MW $<$ 0.4 kDa) could be hardly adsorbed on the carbon nanotubes. Amirbahman *et al.*[41] reported that HA filtered through larger molecular weight cut-off (MWCO) membranes afforded better stability for hematite nanoparticles against deposition. Similar results have been observed when studying the influence of molecular weight fractionated NOM on the aggregation of fullerene,[42] gold nanoparticles,[43] and the photo-reduction of Ag^+ to silver nanoparticles.[44] In these studies, the stability of ENPs were considerably enhanced as the adsorbed HA effectively increased electrostatic and/or steric repulsive forces between nanoparticles. Overall, these findings significantly highlighted the important roles of different HA fractions in the fate and transport of ENPs. Nevertheless, to the best of our knowledge, there is no comprehensive study that has investigated the influence of MW fractionated humic acid (M_f-HA) on the transport and retention of ENPs.

Quantum dots (QDs), as a kind of ENP, have been well-known for their distinguished tunable optical properties and are widely used in solar cells, biomedical imaging, luminescent probes, chemical analysis, display and lighting technologies.[45,46] In this study, we used QDs as a type of ENP to understand the effects of different MW fractions of humic acid on the transport and retention of nanoparticles. A series of column experiments with two differently coated QDs in the presence of mono- or divalent electrolytes and with or without pristine- or M_f-HA were performed. Additionally, the characteristics of pristine- and M_f-HA and the potential and size of the QDs under various conditions were fully investigated. To date, this is the first study on the influence of MW distribution and heterogeneity of HA on the transport and retention of QDs.

2. Materials and methods

2.1 Fractionation and characterization of humic acid

Humic acid (Lot No. 1415936) was obtained from Sigma-Aldrich (Shanghai, China). The stock solution (1 g L^{-1}) was stirred overnight at room temperature and then filtered through a 0.22 μm pore-size hydrophilic polyvinylidene fluoride (PVDF) membrane to prevent any undissolved HA. The filtrate is referred to as pristine-HA. A series of nominal molecular weight cut-off (MWCO) Amicon Ultra-15 centrifugal filters (100, 30, 10, and 3 kDa, respectively) obtained from Millipore (Darmstadt, Germany) were used to fractionate HA. The procedure of fractionating HA followed the protocol

reported by Yin *et al.*[47] Briefly, all filter units were initially rinsed with deionized (DI) water to remove glycerol thoroughly. Next, the pristine HA was loaded into the 100 kDa filter and centrifuged at 3737 g for 30 min. The filtrate was collected without any modification and then further filtered stepwise using 30 kDa, 10 kDa, and 3 kDa filters at centrifugation rates of 5090 g, 6650 g, and 8420 g, respectively. The retentate or filtrate was collected as M_f-HA (>100 kDa, 30–100 kDa, 10–30 kDa, 3–10 kDa, and <3 kDa, respectively). The carbon weight percent (wt%) recovery of M_f-HA was 91.0% (ESI† Table S1), indicating that 9% of HA could be lost to the filter membrane during the washing process.[48]

Concentrations of the pristine HA and M_f-HA were quantified as total organic carbon (TOC) using a Shimadzu TOC-V Analyzer. UV-vis spectrophotometric analysis spectra and fluorescence excitation–emission matrices (EEMs) were comprehensively obtained for the characterization of pristine- and M_f-HA. The concentration of HA used in the UV-vis and fluorescence analyses was 5 mg L^{-1} dissolved organic carbon (prepared in DI water and adjusted to pH 7.0 with 0.1 M HCl and 0.1 M NaOH). UV-vis spectra were measured using a Shimadzu UV-vis NIR spectrophotometer (UV-3600, Japan). Fluorescence excitation–emission matrices (EEMs) were obtained on a Hitachi fluorescence spectrophotometer (F-4600, Japan) with a 1 cm quartz cuvette. Both excitation and emission slit widths were set to 5 nm. Emission was measured from 280 to 600 nm in 10 nm increments, with excitation wavelengths in the range of 200 to 450 nm in 10 nm increments.

2.2 Preparation and characterization of the nanoparticles

Two types of QDs were used in this study: carboxyl-functionalized CdSe/ZnS QDs (Wu Han Jia Yuan, Catalog No. Q2525) and amine-functionalized CdSe/ZnS/PEG QDs (Wu Han Jia Yuan, Catalog No. Q4525). Their emission wavelength is 525 nm and particle diameter is 12–18 nm. The QDs were shipped in borate buffer solution (BBS) at 8 μM. To investigate the potential effects of humic acid heterogeneity on the transport behavior of QDs, QD suspensions were prepared by diluting the QD stock solution with a variety of background solutions (3 mM NaCl or 2 mM $CaCl_2$ in the presence and absence of pristine- and M_f-HA at pH 7.0). The final concentration of the QD suspensions was 5×10^{12} particles per mL.

The electrophoretic mobility (EPM) of the QDs was measured using a Zetasizer Nano ZS (Malvern Instruments, UK) in a wide range of environmental relevant background solution chemistries. All measurements were conducted in triplicate. The hydrodynamic diameter of the QDs in the desired background solution chemistry was assessed by dynamic light scattering (DLS) (ZetaSizer Nano, Malvern) at a 173° scattering angle. The size of the particles was also determined by transmission electron microscopy (TEM) under selected conditions. The samples prepared using a small drop of QD suspension were placed onto a copper grid with a carbon backing, followed by air drying overnight prior to analysis.[15] The mean sizes of the QDs were determined by the analysis of at least three randomly chosen images recorded and each frame has more than 30 particles.

2.3 Adsorption of HA on the QDs

Adsorption studies were conducted to confirm the adsorbed amount of HA on the QD surface under conditions that were used in the column transport experiments. Immediately after the completion of the QD suspension preparation, 20 mL of the suspension was added into a clean centrifuge tube. The suspensions and colloid-free solutions were stirred for 24 h and then centrifuged for 2 h at 8000 rpm (*ca.* 8520 g) to settle the HA–colloid complex. The HA concentration in the supernatant was measured using a Shimadzu TOC-V analyzer. The difference between the initial and final HA concentrations in the aqueous phase was used to determine the adsorbed amount of HA. The results are reported as mg HA m^{-2}. The complete procedure is provided in the ESI.†

2.4 Column transport experiments

Through column experiments, we firstly studied the individual effects of the mono/divalent electrolyte solutions (3 mM NaCl or 2 mM $CaCl_2$) on the transport of QDs, and then investigated the co-influence of pristine- and M_f-HA with the mono/divalent electrolyte solutions on the transport of QDs. A total of 14 column experiments were conducted following the procedures described in a previous study.[49] To summarize, a glass chromatography column (1.6 cm i.d. × 10 cm length) was wet-packed uniformly with clean sand to avoid introducing air bubbles into the porous media, following mild sonication to achieve maximum packing density. Once packed, the column was equilibrated with at least 10 pore volumes (PVs) of the desired background solution (3 mM NaCl or 2 mM $CaCl_2$ in the presence and absence of pristine- and M_f-HA at pH 7) in the up-flow mode at a flow rate of 1 mL min^{-1} (equivalent to a Darcy velocity of 2.8 m d^{-1}).

After equilibrating with the background solution, nonreactive tracer tests were used to assess the water flow and hydrodynamic dispersion of the packed column. A pulse (*ca.* 3 PVs) of sodium nitrate ($NaNO_3$) solution was introduced at a flow rate of 1.0 mL min^{-1} into the column, followed by 3 PVs of the background solution injected to replace the tracer solution. The concentration of the tracer in the effluent samples was measured using a Shimadzu UV-vis NIR spectrophotometer to obtain the breakthrough curves (BTCs).

Once the tracer tests were completed, a pulse (*ca.* 3 PVs) of QD suspensions with the same background electrolyte compositions was introduced into the column immediately, and then a pulse of the QD-free background solution (*ca.* 3 PVs) was injected to elute the unattached QDs. The effluent samples were collected using a fraction collector and an ICP-OES was used to measure the QD concentration. At the end of each experiment, the columns were carefully sectioned into 1.5 cm increments and the QDs were extracted from

each solid sample and measured to obtain a retention profile.

The concentrations of the QDs were determined using an inductively coupled plasma-optical emission spectrometer (ICP-OES; OptimaTM 7300DV, PerkinElmer, Inc., Shelton, CT, USA) operated at a RF power of 1500 W, a nebulizer flow of 0.8 L min^{-1}, and a pump rate of 1.5 mL min^{-1} at a wavelength of 214.44 nm. The influent and effluent concentrations of the QDs were determined by direct injection into the ICP-OES without pre-treatment. The solid-phase QD concentration was measured using ICP-OES after pre-treatment (dried at 95 °C and digested in 10 mL of nitric acid, using a microwave-assisted digester). The detailed analytical method for different QD concentrations is shown in the study of Wang *et al.*[20]

2.5 Calculation of interaction energy

In order to better understand the influence of different M_f-HA on the transport and retention behaviour of QDs in porous media under various conditions, the Derjaguin–Landau–Verwey–Overbeek (DLVO) theory was modified by the incorporation of a steric repulsive energy term when HA coated QDs approach the sand surface.

In the absence of HA, the interaction energy calculations for the QDs in the electrolytes were only considered classical DLVO interaction energies, including electrical double layer (EDL) repulsion and van der Waals (VDW) attraction forces. In the presence of HA, the steric repulsion forces including osmotic repulsion (V_{osm}) and elastic-steric repulsion (V_{elas}) forces were also considered in the interaction energy calculations. The QD–sand interaction energy was calculated by treating the particle-collector system as a case of sphere–plate interaction. The total interaction energy is the sum of these forces and the steric repulsion forces only considered when HA existed in the QD suspension. As the coating of particles or the presence of any hydrated ions will prevent the surface–surface separation distances approaching x = 0.3 nm,[50] the interaction forces were intentionally calculated for $x > 0.3$ nm. This also resulted in the interaction energy profiles structures not exhibiting a primary minimum. The detailed equations used to calculate electrical double layer repulsion (eqn (S7) in the ESI†), van der Waals attraction forces (eqn (S6) in the ESI†) and steric repulsion energies (eqn (S10)–(S14) in the ESI†) for the QD–sand interaction are provided in the ESI.†

2.6 Interpretation of nanoparticle transport experiments

In order to quantitatively compare the transport behavior of QDs under different experimental conditions, the particle attachment efficiency (α) based on the colloid filtration theory was calculated following the expression:[51]

$$\alpha = -\frac{2}{3}\frac{d_c}{(1-\varepsilon)L\eta_0}\ln\left(\frac{C}{C_0}\right) \quad (1)$$

where, d_c is the mean diameter of the collector grain, ε is the porosity of the packed-bed, L is the packed-bed length and C/C_0 represents the normalized particle effluent concentration. The value of C/C_0 was determined by numerical integration of the measured particle breakthrough curve for each experiment. η_0 is the single-collector contact efficiency. The value of η_0 was determined using the correlation equation reported by Tufenkjie and Elimelech.[51]

2.7 Data analysis

The zeta potential and particle size data were analysed using one-way ANOVA (Tukey's honestly significant difference (HSD) test) to identify the statistical differences in the measured parameters (HA MW). In addition, a linear regression analysis was also performed using the average MW for each HA fraction to identify the correlation between the HA MW and zeta potential or particle size of the QDs. The significance was set to $p < 0.05$. All tests were performed using the IBM SPSS Statistics version 23 software package.

3. Results and discussion

3.1 Chemical characterization of pristine- and M_f-HA

The UV-vis spectra, specific UV absorbance at 280 nm (positively correlated to aromaticity) and $E_2:E_3$ (absorbance at 250 and 365 nm) for pristine- and M_f-HA are presented in Fig. 1a–c, respectively. All humic samples demonstrated a featureless decrease in absorbance with increasing wavelength. The ratio of E_2/E_3 was increasing with the decrease in the molecular weight of HA. The absorbances at 280 nm of the >100 kDa and 30–100 kDa HA fractions were higher than those of other fractions. These results indicated that the higher MW M_f-HA had more aromatic components and hydrophobic structures.[44,47]

Fig. 1d–i shows the fluorescence excitation–emission matrices of pristine-HA and M_f-HA. The maximum intensity of the fluorescence peaks was more pronounced for the low MW M_f-HA (10–30 kDa, 3–10 kDa and <3 kDa HA) than those for the high MW M_f-HA (>100 kDa and 30–100 kDa HA). As the humic-like fluorescence is mainly caused by carboxylic groups,[42] the results demonstrated an abundance of carboxylic functional groups existing in the low MW M_f-HA (10–30 kDa, 3–10 kDa, and <3 kDa HA). Previous studies observed similar results wherein the low MW fractions of NOM had more carboxyl groups while the high MW fractions contained more aromatic structures.[42,47]

3.2 Zeta potentials and sizes of QDs in the absence and presence of pristine- and M_f-HA

The measurements of the ζ potentials and size of the QDs were performed with carboxyl and amino modified QDs to gain an insight into the surface potential behavior imparted by each molecular weight HA in the mono- and divalent electrolytes. Fig. 2 shows the zeta potentials and sizes of QDs under different solution chemistry conditions. In the absence

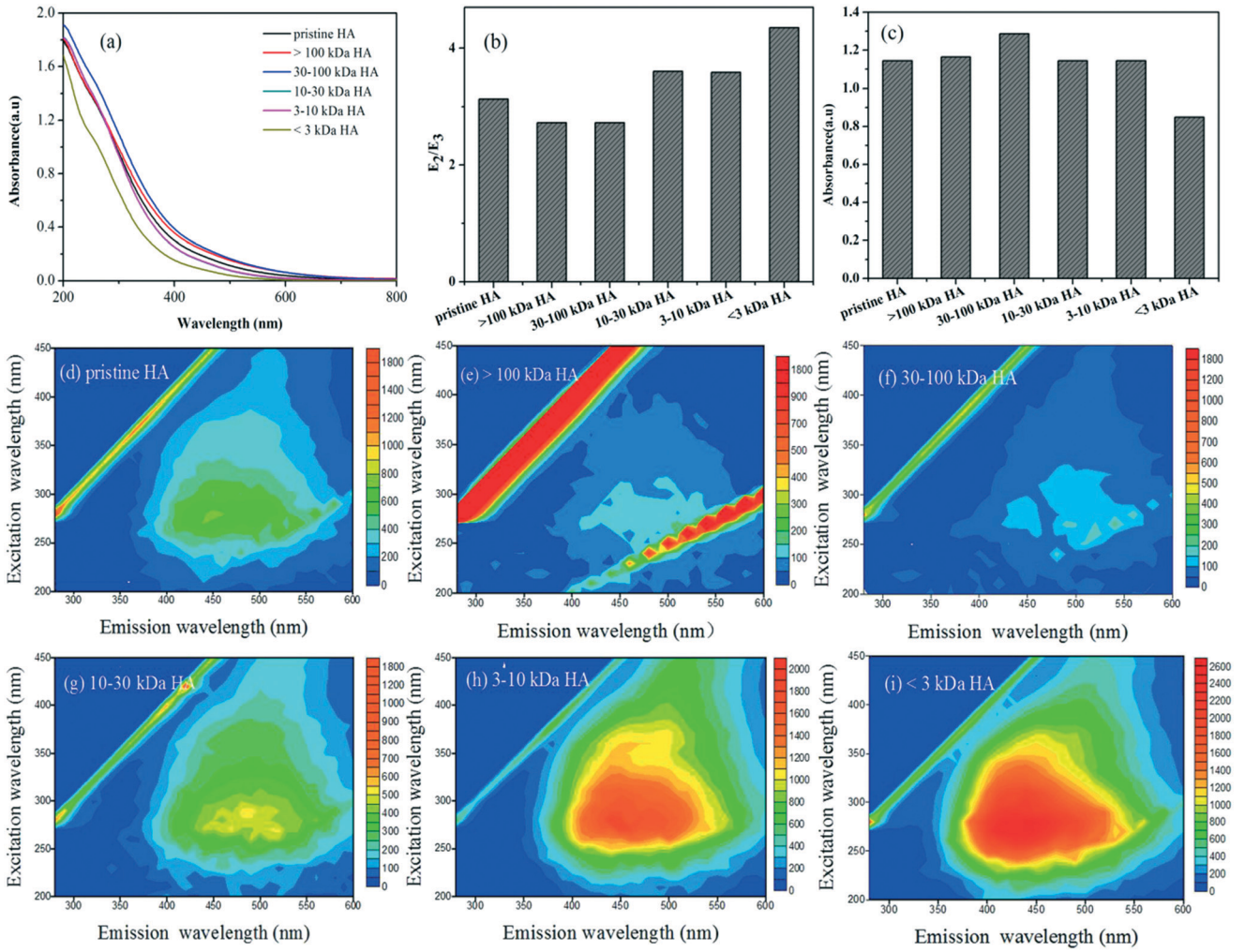

Fig. 1 (a) UV-vis spectra, (b) the quotient of absorbance values at 250 nm and 365 nm (E_2/E_3), (c) the absorbance values at 280 nm for pristine- and M_f-HA, and (d–i) fluorescence EEMs for pristine-HA and M_f-HA.

of HA, the ζ potentials of QD–COOH were more negative in the NaCl solution than those in the $CaCl_2$ solution, while QD–NH_2 had more positive charges in the $CaCl_2$ solution than those in the NaCl solution. The aggregation size of QDs in the monovalent electrolyte was less than those in the divalent electrolyte, which indicated that the QDs were more stable in monovalent electrolyte than in divalent electrolyte.

In the presence of 3 mg L^{-1} pristine- and M_f-HA, the ζ potentials of the QDs were more negative relative those in the absence of HA, and the aggregation of the QDs was inhibited by pristine- and M_f-HA under most conditions. However, the effect of the HA MW on the ζ potentials and sizes of the two QDs were notably different. In the NaCl electrolyte, the ζ potentials of QD–COOH in the presence of the M_f-HA was more negative relative to those without HA, but the variation in the measured ζ potentials of QD–COOH was not significantly correlated with the MW of the M_f-HA. In contrast, the effect of the HA MW on the ζ potentials of QD–COOH in the $CaCl_2$ solution was significantly correlated with the HA MW (ESI† Table S2). The ζ potential of QD–COOH was more negative in the presence of the low MW HA fractions (10–30 kDa, 3–10 kDa and <3 kDa HA) than that in the high MW HA fractions (>100 kDa and 30–100 kDa HA). However, the aggregation of QD–COOH in the divalent electrolyte was inhibited by high MW M_f-HA (>100 kDa and 30–100 kDa HA) more efficiently than by low MW M_f-HA (10–30 kDa, 3–10 kDa and <3 kDa HA). It seems that, while the low MW HA contained more carboxyl groups (Fig. 1) and could impart more negative charges to the QDs, it does not contribute to the stability as much as the high MW HA. High MW M_f-HA can impart stronger steric repulsion to QDs than low MW M_f-HA, which resulted in better dispersion of QD–COOH in high MW HA. Interestingly, the aggregation of QD–COOH in the monovalent electrolyte was slightly enhanced by pristine- and M_f-HA (except the fraction of >100 kDa HA). The aggregation of nanoparticles is usually determined by electrostatic and steric repulsion. A previous study[47] has reported that high MW NOM possibly enhanced the aggregation of PVP-AgNPs through screening the surface coating of PVP thus reducing the steric repulsion, while the zeta potentials of PVP-AgNPs were higher in the

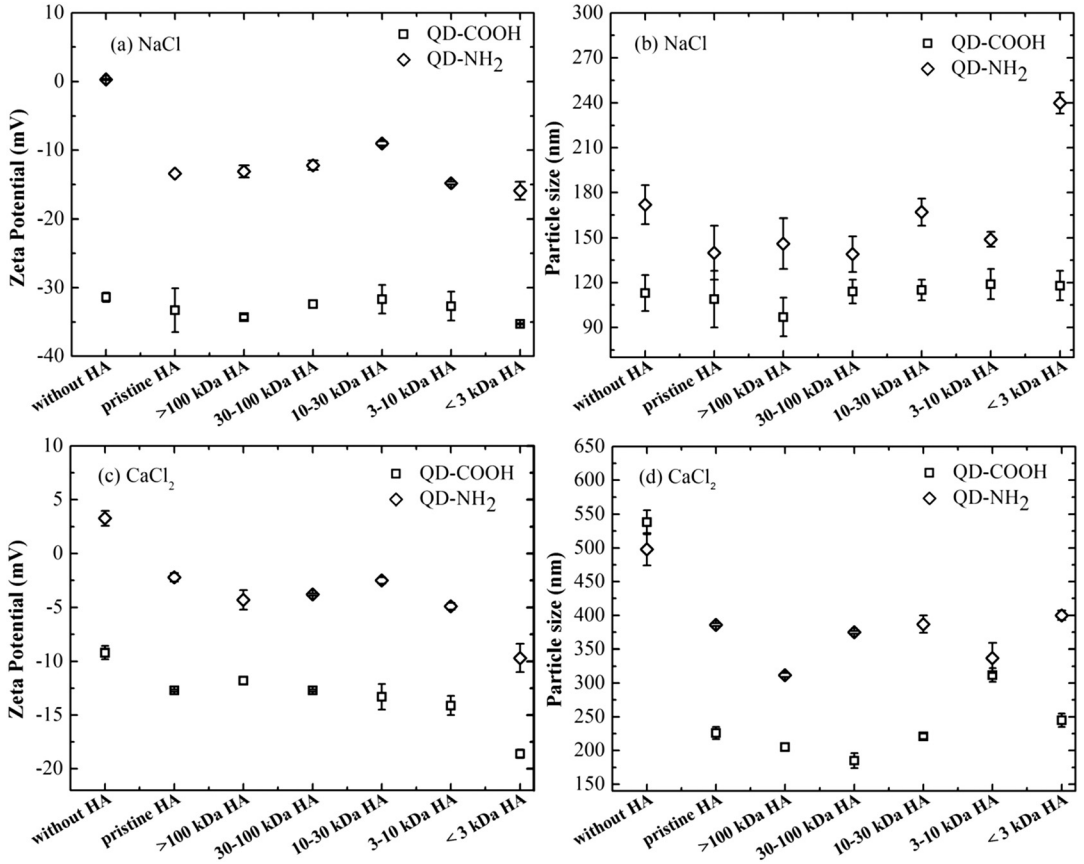

Fig. 2 Zeta potentials (a and c) and particle size (b and d) of QDs in the absence and presence of pristine- and M_f-HA in 3 mM NaCl or 2 mM $CaCl_2$ solutions.

presence of high MW NOM. Thus, in this study, although the overcoating or replacement of HA increased the interparticle electrostatic repulsion, it possibly reduced the steric repulsion by screening the surface coating of QD–COOH, which resulted in minor aggregation of QD–COOH in this case.

Compared with QD–COOH, the ζ potentials of QD–NH_2 in the presence of pristine- and M_f-HA were changed highly relative to the pristine particles (without HA in the suspension). However, the HA MW has little further effect on the ζ potentials of QD–NH_2. The effect of each MW fraction of HA on the ζ potentials of QD–NH_2 was not significant (ESI† Table S3). The aggregation of QD–NH_2 both in mono- and divalent electrolytes was inhibited by pristine- and M_f-HA. High MW M_f-HA could inhibit the aggregation of QD–NH_2 much better than low MW M_f-HA in the monovalent electrolyte. It is noted that the effect of each MW fraction of HA on the aggregation size of QD–NH_2 in divalent electrolyte was significant (ESI† Table S3) and the correlation between the aggregation size of QD–NH_2 and HA MW was weak. In general, the above observed results indicate that while low MW HA imparts more negative charges (contained more carboxyl groups) to QDs in most cases, it does not contribute to the stability as much as high MW HA, likely because of the more significant steric effects that high-MW HA has on the stability against homoaggregation.

3.3 Effects of the molecular weight of humic acid on the transport and retention of QDs in the sand porous media

3.3.1 Effects of pristine- and M_f-HA on the transport and retention of QDs in monovalent electrolyte. The transport and retention behaviour of QDs in quartz sand both with and without pristine- and M_f-HA in suspensions were first investigated in NaCl solution at pH 7, and the corresponding breakthrough curves and retention profiles (RPs) are presented in Fig. 3 and 4. The data on pristine and >30 kDa HA coated QDs are shown in (a) and (c) and that <30 kDa fractions are shown in (b) and (d). The BTCs are plotted as the normalized particle concentration at the column effluent (C/C_0) *versus* the number of PVs that passed through the column. The RPs are given as the normalized solid-phase concentration (S/C_0) against column depth.

As shown in Fig. 3, very similar breakthrough curves and retention profiles were obtained for QD–COOH in NaCl solution with or without HA in the suspensions. Compared to the transport results, the mobility of QD–COOH was significant in the monovalent electrolyte. A similar observation was obtained in previous studies where QD–COOH was highly mobile in the sand column with the monovalent electrolyte.[16,19,23] Interestingly, in the absence of HA, the transport of QD–COOH was retarded. QD–COOH suspended in 3 mM NaCl appeared in the effluent after 1.0 PVs, while the mass

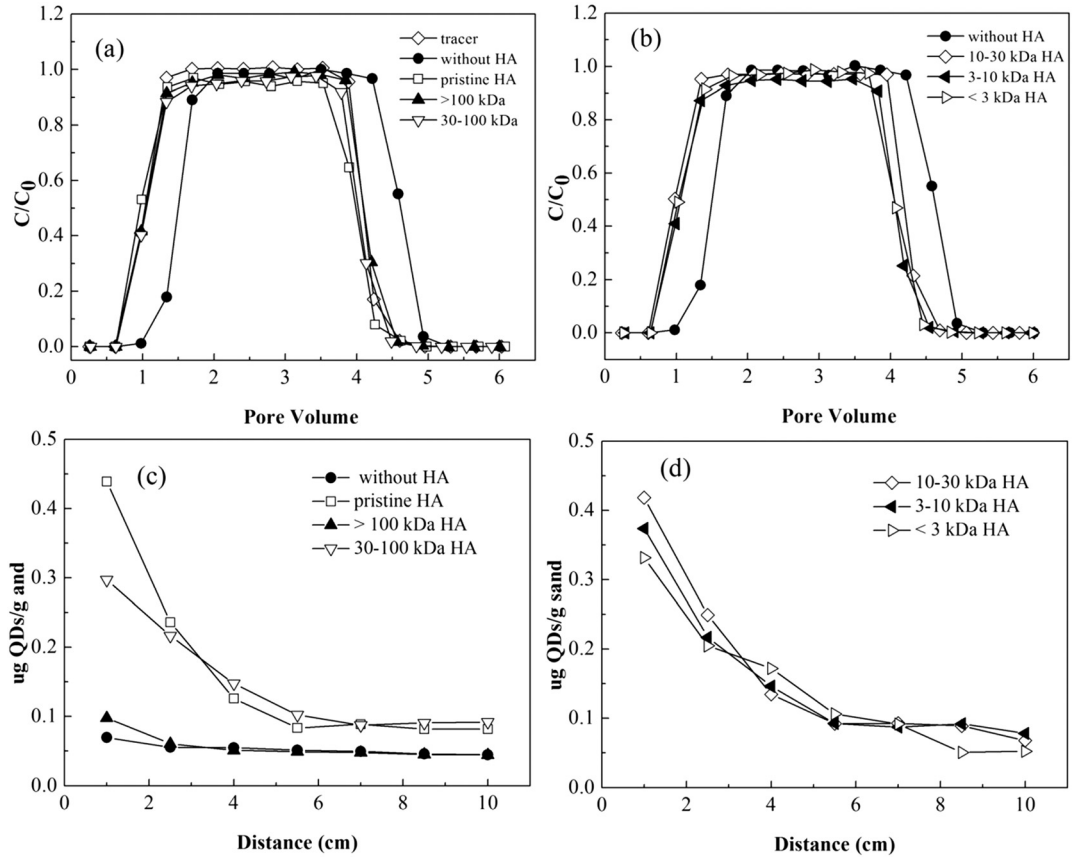

Fig. 3 Effluent breakthrough curve (a and b) and retention profiles (c and d) obtained for QD–COOH transport in quartz sand at 3 mM NaCl with/without pristine- and M_f-HA at pH 7.0.

recovery of QD–COOH in the effluent was close to100% (ESI† Table S4). This may be attributed to their reversible attachment/detachment to the media when moving through the column. The retention profile of QD–COOH without HA in the suspension revealed a low retention of QD–COOH in sand. This was in good agreement with what the DLVO calculations (ESI† Fig. S1) predicted, which indicated that the sand surface was unfavorable for particle deposition.

It is noted that the effects of pristine- and M_f-HA on the transport and retention of QD–COOH were not significant in the NaCl solution. Although QD–COOH was highly mobile in the sand column, the mass recovery of QD–COOH in the effluent was slightly decreased relative to that without HA (ESI† Table S4). And this decrease was not related to the MW of HA. Similarly, the retention profiles (Fig. 3c and d) and attachment efficiency of QD–COOH (Fig. 7) in the presence of pristine- and M_f-HA were higher than those without HA. In an attempt to better explain these observations, the interaction energy between the QDs and the sand was calculated at each condition (Table 1). The DLVO energy calculations were modified by the incorporation of steric repulsion energy (osmotic repulsion and elastic-steric repulsion) when HA coated QDs approach the sand surface. The modified interacting energy profiles for QD–COOH and sand with the monovalent electrolyte are presented in ESI† Fig. S2. The modified DLVO interaction energy calculations (ESI† Fig. S2) revealed the presence of significant repulsive energy barriers (>128 kT) between the QDs and sand under all conditions, indicating that the QDs appeared unlikely to conquer those energy barriers and are deposited in the primary energy minimum. Previous studies suggested that the secondary energy minimum can be an important mechanism that governed the transport of colloids in porous media.[52,53] As seen in Fig. S2,† the interaction energy profiles also showed the existence of a very shallow secondary energy minimum under all conditions. The calculated values of the secondary energy minimum presented in Table 1 showed that the secondary energy minimum was deeper in the low MW HA fractions than that in the high MW HA fractions. Because otherwise there would be a relation between mobility and MW in the column experiments, this suggested that the secondary energy minimum was not the main mechanism that governed the transport of QD–COOH in this condition.[54] Moreover, surface charge heterogeneity could also influence the transport of nanoparticles. Previous studies[54,55] have also reported that the presence of surface charge heterogeneity in sand could produce local areas of favorable interaction, which could increase colloid attachment even under

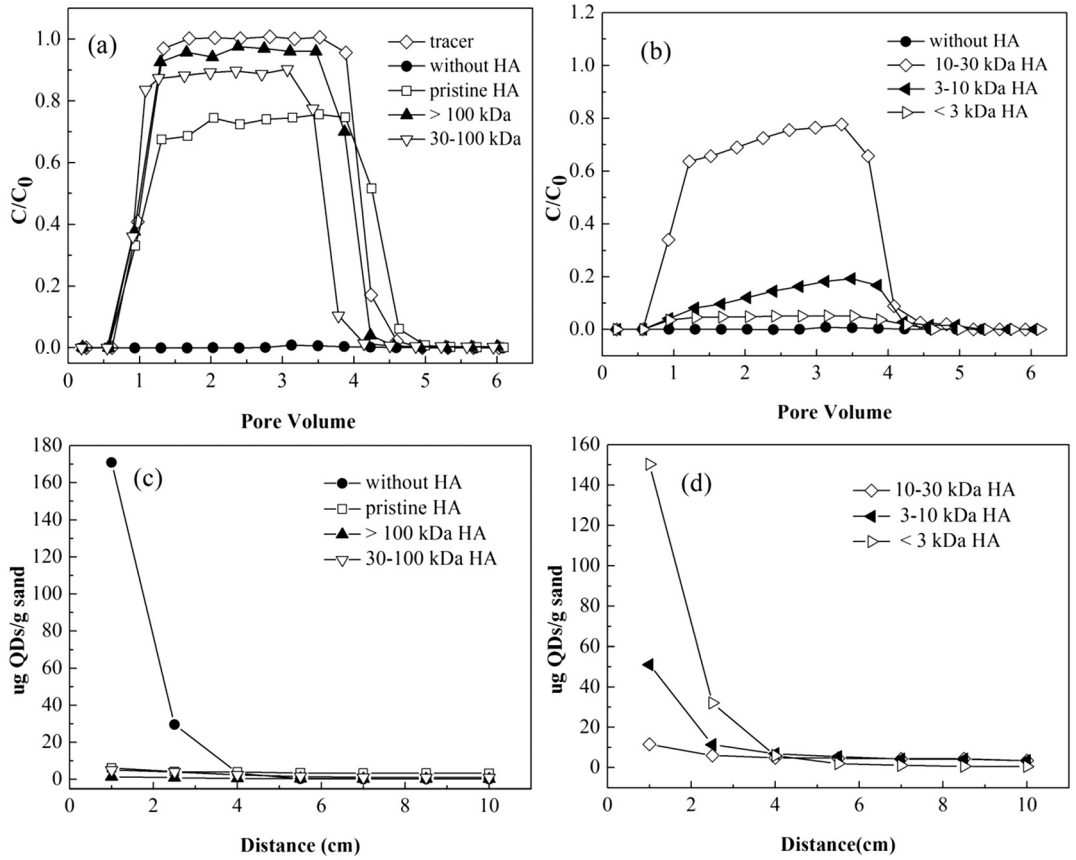

Fig. 4 Effluent breakthrough curve (a and b) and retention profiles (c and d) obtained for QD–NH_2 transport in quartz sand at 3 mM NaCl with/without pristine- and M_f-HA at pH 7.0.

unfavorable conditions. The quartz sand used in this study was thoroughly cleaned to remove surface charge heterogeneity, but nanoscale charge heterogeneities from the sand surfaces cannot be ruled out completely. Therefore, a very small amount of QD–COOH deposition in the presence of HA may occur due to the presence of the secondary energy minimum and/or other mechanisms such as surface charge heterogeneities.[22]

As seen in Fig. 4, the transport and retention behavior of QD–NH_2 in the porous media were different to those of QD–COOH. QD–NH_2 was nearly deposited on the sand with 3 mM NaCl solution without HA, which most likely resulted from the strong electrostatic attraction force between the positive potential of QD–NH_2 and the negative potential of the sand. However, QD–NH_2 suspended in pristine HA and NaCl was highly mobile in the sand as evidenced by the high recovery and low retention (Table S4†). The BTCs of the QDs reached a peak value of C/C_0 = 0.74 after 2 PVs, and 26% of the injected QDs were retained in the sand. It has been reported that HA could increase particle stability and decrease rates of attachment.[31,56,57] Similar observations showed that HA enhanced the transport of $nTiO_2$ (ref. 52) and fullerene (C_{60}) nanoparticles.[25] In addition, HA can adsorb on the surface of the particles and alter the electrostatic property, thus increasing the electrostatic repulsion and providing more steric force to stabilize nanoparticles in the aquatic environment.[56]

In the presence of M_f-HA, the mobility of QD–NH_2 in the monovalent electrolyte was significantly enhanced. Generally, this enhanced effect was strongly related to the MW of M_f-HA. The high MW M_f-HA enhanced the mobility more significantly than the low MW M_f-HA. Such MW-dependent effect on the nanoparticle stability by M_f-HA was also observed in previous studies.[42,47] The injected QDs were significantly transported across the column in the presence of the high MW HA fractions (>100 and 30–100 kDa HA), while the effluent concentration of the QDs reached a peak value of C/C_0 = 0.05 in the presence of <3 kDa HA. The retention of QD–NH_2 with the low MW HA fractions (30–10 kDa, 3–10 kDa, and <3 kDa HA) and NaCl in the suspensions was higher than that in the presence of the high MW HA fractions in the suspensions. In addition, the value of the attachment efficiency of QD–NH_2 increased with the decrease in MW (Fig. 7). These observations indicated that the high MW HA fractions could enhance the mobility of QD–NH_2 in the monovalent electrolyte more efficiently than low MW HA. Compared with QD–COOH, the influence on the transport of QD–NH_2 was more efficient with the same MW M_f-HA, indicating that the role of surface coating of particles is also important in the transport behaviour of nanoparticles. The adsorption studies revealed

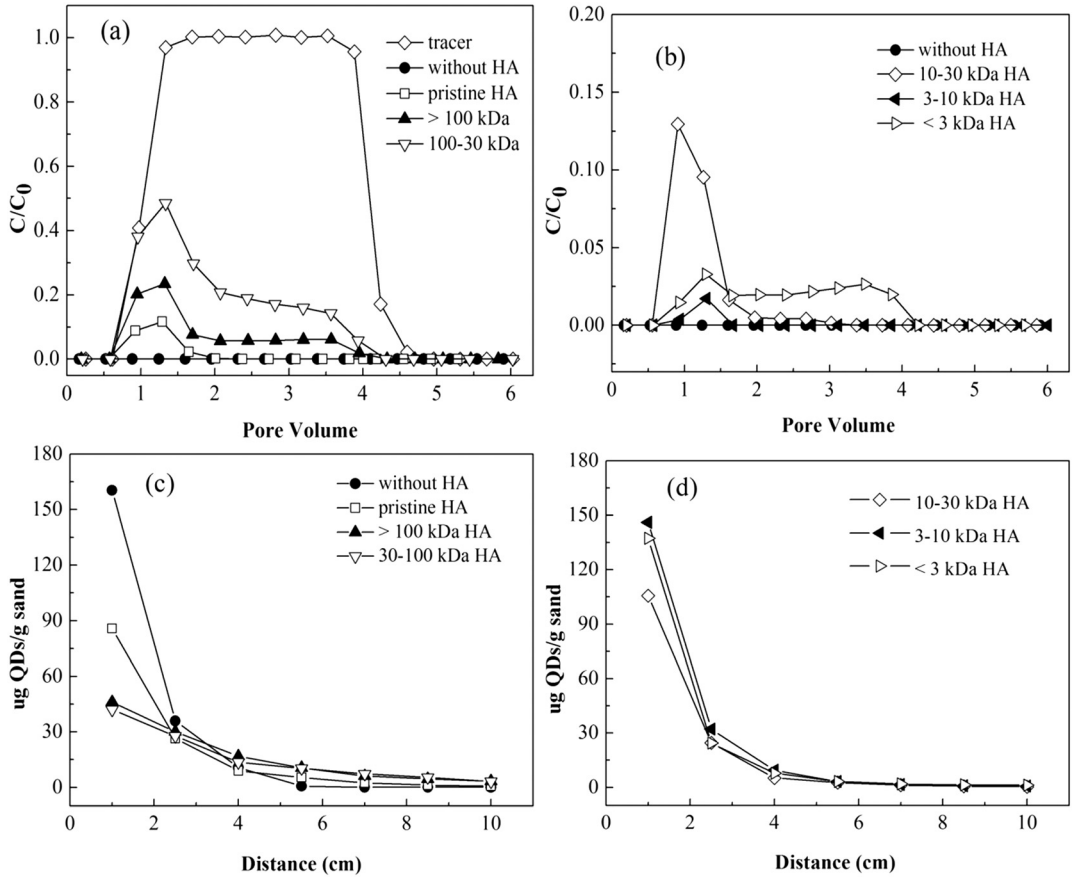

Fig. 5 Effluent breakthrough curve (a and b) and retention profiles (c and d) obtained for QD–COOH transport in quartz sand at 2 mM $CaCl_2$ with/without pristine- and M_f-HA at pH 7.0.

that the adsorbed amount of HA on the QD–NH_2 surface increased with the increase of the HA MW (ESI† Table S5). The adsorbed HA on the surface of the nanoparticles could impart more electrostatic forces and steric repulsion forces to particles. Table 1 shows that the steric repulsion energy in high MW M_f-HA was higher than that in the low MW M_f-HA fractions, and the height of the energy barrier in the high MW HA fractions (>100 kDa and 30–100 kDa HA) was higher than that in the low MW HA fractions (10–30 kDa, 3–10 kDa and <3 kDa HA) after incorporation of the steric repulsion energy into the DLVO calculations. These results indicated that the high adsorption and strong steric repulsion[47] of the high MW M_f-HA could explain the aforementioned MW-dependent effect (the high MW HA fractions could enhance the mobility of QD–NH_2 in the monovalent electrolyte more efficiently than the low MW HA). Furthermore, the modified DLVO interaction energy profiles (ESI† Fig. S3) showed that the secondary energy minimum in the low MW HA fractions (10–30 kDa, 3–10 kDa and <3 kDa HA) was deeper than that in the high MW HA fractions (>100 kDa and 30–100 kDa HA). This suggests that the secondary minimum is likely an important mechanism for the obtained transport behavior of QD–NH_2. Nonetheless, how the component (the composition of each MW fraction of HA) interacted with the surface coating of the nanoparticles in this enhanced transport is still not clear. Further studies should investigate how a specific component influences the transport and fate of nanoparticles.

3.3.2 Effects of pristine- and M_f-HA on the transport and retention of QDs in the divalent electrolyte. The transport and retention behavior of the QDs were also studied in divalent electrolytes. Fig. 5 and 6 show the observed BTCs and RPs of QD–COOH and QD–NH_2, respectively. Compared with Fig. 3a, QD–COOH was significantly deposited on the sand in 2 mM $CaCl_2$. Other studies[19,22] which investigated the transport and retention of QDs have also reported relatively high deposition rates on sand. The DLVO calculations (ESI† Fig. S1) suggested the presence of a high energy barrier (26.14 kT) and a deep secondary energy minimum (−0.0050 kT) between QD–COOH and the sand. This suggested a higher energy barrier against QD–COOH deposition in the primary energy minimum, while QD–COOH can be captured in the secondary energy wells.[58] Moreover, it has been reported that the divalent cations could decrease the surface potential through screening the particle charge and forming divalent cation (Ca^{2+}) bridges between the negatively charged QDs and the negatively charged sand surfaces.[59] Thus, the significant deposition of QDs in the presence of Ca^{2+} is likely due to the formation of cation bridges between the QDs and surface and the secondary energy minimum.

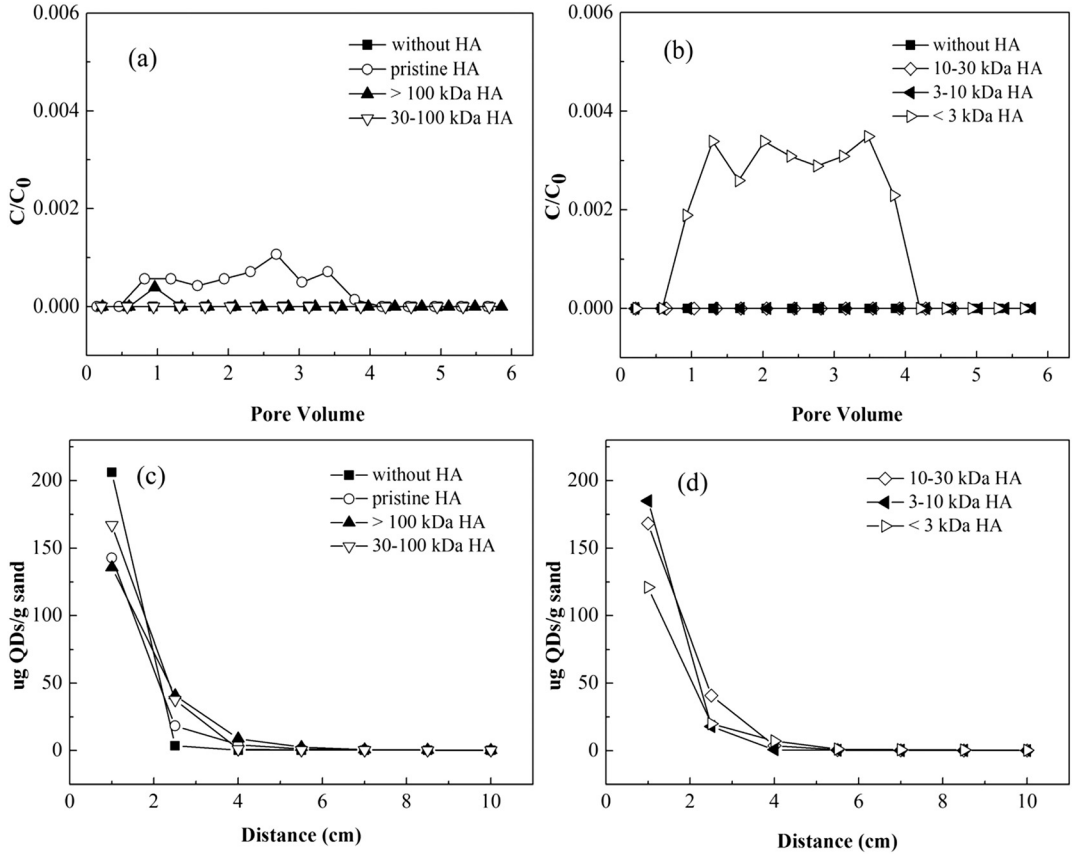

Fig. 6 Effluent breakthrough curve (a and b) and retention profiles (c and d) obtained for QD–NH_2 transport in quartz sand at 3 mM $CaCl_2$ with/without pristine- and M_f-HA at pH 7.0.

Furthermore, Fig. 5a also shows that the pristine- and M_f-HA had distinct effects on the transport and retention of QD–COOH in divalent electrolytes. All the HA enhanced the mobility of the QDs in the sand column. In the presence of pristine HA, the BTCs of QD–COOH rapidly increased to a maximum peak value and then slowly decreased. Moreover, the BTCs of QD–COOH nearly coincided with that of the nonreactive tracer. Similar BTC shapes were also observed in the presence of M_f-HA. Compared with the monovalent electrolyte, the transport of QD–COOH in divalent electrolytes was more sensitive to the changes in the MW of M_f-HA. All the M_f-HA enhanced the mobility of the QDs in the sand column, and the high MW HA fractions (>100 kDa, 30–100 kDa HA) facilitated the transport of the QDs in the $CaCl_2$ solution more significantly than the lower MW HA fractions (3–10 kDa, and <3 kDa HA). Moreover, the retention profile of QD–COOH with M_f-HA in the suspension was lower than that without HA, while the shapes of the retention profiles of QD–COOH with HA in the suspensions were similar to those without HA in the suspensions. This result suggested that the presence of HA in the QD–COOH suspensions may not change the deposition mechanisms of QD–COOH in the sand with divalent electrolytes.[60] However, these observations were in good agreement with the modified DLVO interaction energy profiles (ESI† Fig. S4) predicted. The height of the energy barrier in the high MW HA fractions (>100 kDa and 30–100 kDa HA) were higher than that in the low MW HA fractions (10–30 kDa, 3–10 kDa and <3 kDa HA), while the secondary energy minimum was deeper in the low MW HA fractions than in the high MW HA fractions. In addition, the secondary energy minimum is less deep for the 3 kDa than for the 3–10 kDa HA, this was also reflected in the transport behavior of QD–COOH in Fig. 5b. These results suggested that the

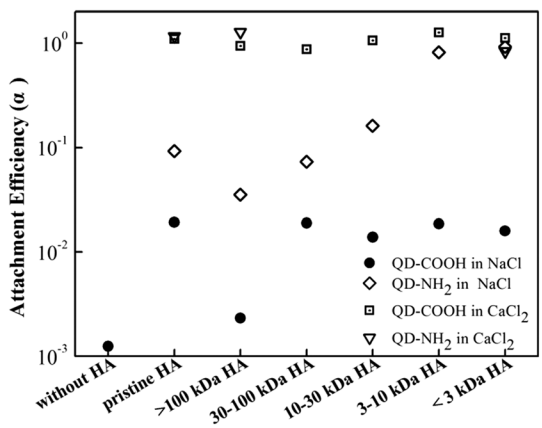

Fig. 7 The average attachment efficiencies for QDs suspended in NaCl and $CaCl_2$ solutions.

Table 1 Calculated steric repulsion forces, maximum energy barriers, secondary minimum depths and distances for QDs interacting with the sand in the presence/absence of pristine- and M_f-HA in mono- and divalent electrolytes

Electrolyte	Particle	HA type	Steric repulsion (kT)	Φ_{max} (kT)		Φ_{min}	
				DLVO	Modified DLVO	Depth (kT)	Distance (nm)
NaCl	QD–COOH	Without HA	—	87.26	—	−0.0047	62
		Pristine HA	19.89	123.40	138.77	−0.0044	70
		>100 kDa HA	41.18	105.05	144.27	−0.0039	68
		30–100 kDa HA	35.10	128.72	155.40	−0.0045	70
		10–30 kDa HA	33.02	97.94	128.24	−0.0049	68
		3–10 kDa HA	32.28	125.76	153.97	−0.0048	68
		<3 kDa HA	24.46	129.20	154.66	−0.0048	70
NaCl	QD–NH_2	Without HA	—	—	—	—	—
		Pristine HA	54.29	30.39	54.67	−0.0066	62
		>100 kDa HA	113.49	29.97	81.73	−0.0070	60
		30–100 kDa HA	107.17	23.96	56.78	−0.0067	60
		10–30 kDa HA	74.29	15.93	55.09	−0.0092	54
		3–10 kDa HA	19.22	39.04	46.77	−0.0071	62
		<3 kDa HA	15.37	48.00	51.88	−0.0075	64
$CaCl_2$	QD–COOH	Without HA	—	26.14	—	−0.0050	64
		Pristine HA	154.45	32.54	154.55	−0.0087	72
		>100 kDa HA	212.57	32.43	225.54	−0.0083	72
		30–100 kDa HA	183.84	26.89	194.62	−0.0067	72
		10–30 kDa HA	61.97	28.90	74.86	−0.0083	70
		3–10 kDa HA	50.99	40.07	76.68	−0.0118	70
		<3 kDa HA	50.94	47.68	88.16	−0.0086	74
$CaCl_2$	QD–NH_2	Without HA	—	—	—	—	—
		Pristine HA	100.51	0.83	45.53	−0.0107	54
		>100 kDa HA	153.08	7.63	81.02	−0.0195	60
		30–100 kDa HA	149.01	6.30	59.33	−0.0206	60
		10–30 kDa HA	55.30	2.24	12.93	−0.0227	54
		3–10 kDa HA	55.20	8.41	36.36	−0.0181	60
		<3 kDa HA	54.56	38.94	82.03	−0.0191	70

secondary energy minimum was an important mechanism for the QD transport. Moreover, adsorption studies also revealed that the amount of adsorbed HA on the QD–COOH surface was higher in the presence of high MW HA than that in low MW HA (ESI† Table S5). This preferential adsorption of high MW NOM was also observed on mineral solid surfaces by ^{13}C-nuclear magnetic resonance and size exclusion chromatography analyses.[61,62] The adsorption of HA could provide additional electrostatic repulsion and steric repulsion, and the steric repulsion provided by high MW was stronger than that provided by low MW HA fractions, which resulted in the higher recovery of QDs in the presence of higher MW M_f-HA.

In contrast, with $CaCl_2$ as the background electrolyte, the mobility of QD–NH_2 was not significantly influenced by the pristine- and M_f-HA. QD–NH_2 was completely deposited on the sand under most conditions. In particular, the transport of QD–NH_2 was slightly enhanced by the pristine HA and <3 kDa HA fraction, but the enhancement was negligible. The retained concentration of QD–NH_2 decreased significantly with the increasing transport distance in the presence of pristine- and M_f-HA. Moreover, the shapes of the retained profiles for QD–NH_2 were similar under all examined conditions, indicating that the deposition mechanism was similar in divalent electrolytes. Although the adsorption of HA changed the chemical properties of QD–NH_2 and enhanced the electrostatic repulsion and between QD–NH_2 and sand, the presence of Ca^{2+} could also form cation bridges between the HA and sand or HA and HA. The modified DLVO interaction energy calculations (ESI† Fig. S5) predicted the presence of a >12 kT primary energy maximum and a deeper secondary energy minimum in the presence of HA. In addition, the height of the energy barrier in the presence of <3 kDa was higher than that in other MW HA and the depth of the secondary energy minimum in pristine HA was less than that in other conditions. This may result in a small amount of QD–NH_2 moving through the column when the fraction of <3 kDa HA or pristine HA existed in the suspensions. It is noted that the depth of the secondary energy minimum in this condition (QD–NH_2 suspended in divalent electrolytes with or without pristine and M_f-HA) was deeper than that in other conditions that have been examined in this study. This suggested that QD–NH_2 is much more likely deposited in the secondary than in the primary energy minimum. The significant deposition of QD–NH_2 in the presence of HA may account for the lower energy barriers and a deeper secondary energy minimum.

In a word, these results for M_f-HA on the transport and retention of COOH– and NH_2–QD in mono- and divalent electrolytes indicated that the coating agent, cation type and M_f-HA have a great influence on the transport of QDs in sand. Generally, high MW M_f-HA could enhance

the mobility of QDs more obviously than low MW M_f-HA. This MW-dependent effect was ascribed to the amount of adsorbed HA on the surface of QDs being higher in the presence of high MW M_f-HA than that in the presence of the low MW HA fractions, and the steric repulsion from high MW M_f-HA was stronger than that from low MW M_f-HA. However, HA cannot govern the transport behaviors of QDs under some conditions. The solution chemistry and particle coating (*e.g.* carboxyl and amino) were also important for the transport and fate of nanoparticles reported in previous studies. The different transport behaviors for QDs in porous media also suggested the importance of the cation type and particle coating on the transport of QDs in the environment.

Conclusions

Understanding the transport and fate of ENPs in a saturated sand column is important to evaluate the potential risk of these materials to environmental and human health. In this study, well-controlled column experiments were conducted using two QDs with different surface functionalities. The results showed that the coating of the QDs has a distinguishing effect on the transport and retention of QDs in both pristine HA and M_f-HA. These findings emphasize that nanoparticles with various coatings will behave differently even under the same conditions. In addition, the results also showed that the different MW fractions of HA play different roles in the transport of QDs. Pristine- and M_f-HA enhanced the transport of carboxyl coated QDs and amino coated QDs in divalent electrolytes and monovalent electrolytes, respectively, and the high MW HA fractions enhanced the transport of QDs more significantly than the low MW HA fractions. Nevertheless, the transport of carboxyl coated QDs in monovalent electrolytes decreased slightly in the presence of pristine- and M_f-HA. The transport of amino coated QDs was not much different in the absence and presence of pristine- and M_f-HA. This molecular weight-dependent effect on the mobility of QDs reveals that different fractions of HA from the natural environment will exhibit many distinguishing effects on the transport and fate of nanoparticles. As the MW component of various sources of HA is very different and physical or chemical processes could also alter the MW distribution of HA from identical sources,[43,63] further studies investigating the effect of the MW composition of different sources of HA on the transport and fate of nanoparticles are highly recommended. Moreover, in order to further thoroughly understand the influence of HA on the transport and fate of nanomaterials, the effects of pH and concentration of M_f-HA should be also investigated in the future.

Conflicts of interest

There are no conflicts of interest to declare.

Acknowledgements

This study was financially supported by the National Natural Science Foundation of China (51521006, 51579099, 51879105 and 51709101), the Program for Changjiang Scholars and Innovative Research Team in University (IRT-13R17), and the Hunan Provincial Innovation Foundation for Postgraduate (CX2016B134).

References

1 L. Qin, G. Zeng, C. Lai, D. Huang, C. Zhang, P. Xu, T. Hu, X. Liu, M. Cheng, Y. Liu, L. Hu and Y. Zhou, *Sens. Actuators, B*, 2017, **243**, 946–954.
2 X. Gong, D. Huang, Y. Liu, G. Zeng, R. Wang, J. Wan, C. Zhang, M. Cheng, X. Qin and W. Xue, *Environ. Sci. Technol.*, 2017, **51**, 11308–11316.
3 J.-H. Deng, X.-R. Zhang, G.-M. Zeng, J.-L. Gong, Q.-Y. Niu and J. Liang, *Chem. Eng. J.*, 2013, **226**, 189–200.
4 J. L. Gong, B. Wang, G. M. Zeng, C. P. Yang, C. G. Niu, Q. Y. Niu, W. J. Zhou and Y. Liang, *J. Hazard. Mater.*, 2009, **164**, 1517–1522.
5 F. Long, J.-L. Gong, G.-M. Zeng, L. Chen, X.-Y. Wang, J.-H. Deng, Q.-Y. Niu, H.-Y. Zhang and X.-R. Zhang, *Chem. Eng. J.*, 2011, **171**, 448–455.
6 P. Xu, G. M. Zeng, D. L. Huang, C. L. Feng, S. Hu, M. H. Zhao, C. Lai, Z. Wei, C. Huang, G. X. Xie and Z. F. Liu, *Sci. Total Environ.*, 2012, **424**, 1–10.
7 C. Zhang, C. Lai, G. Zeng, D. Huang, C. Yang, Y. Wang, Y. Zhou and M. Cheng, *Water Res.*, 2016, **95**, 103–112.
8 Y. Zhang, G. M. Zeng, L. Tang, J. Chen, Y. Zhu, X. X. He and Y. He, *Anal. Chem.*, 2015, **87**, 989–996.
9 C. Zhou, C. Lai, D. Huang, G. Zeng, C. Zhang, M. Cheng, L. Hu, J. Wan, W. Xiong, M. Wen, X. Wen and L. Qin, *Appl. Catal., B*, 2018, **220**, 202–210.
10 P. Xu, G. M. Zeng, D. L. Huang, C. Lai, M. H. Zhao, Z. Wei, N. J. Li, C. Huang and G. X. Xie, *Chem. Eng. J.*, 2012, **203**, 423–431.
11 L. Hu, J. Wan, G. Zeng, A. Chen, G. Chen, Z. Huang, K. He, M. Cheng, C. Zhou, W. Xiong, C. Lai and P. Xu, *Environ. Sci.: Nano*, 2017, **4**, 2018–2029.
12 X. Tan, Y. Liu, G. Zeng, X. Wang, X. Hu, Y. Gu and Z. Yang, *Chemosphere*, 2015, **125**, 70–85.
13 Y. Xiao, K. T. Ho, R. M. Burgess and M. Cashman, *Environ. Sci. Technol.*, 2017, **51**, 1357–1363.
14 S. Tripathi, D. Champagne and N. Tufenkji, *Environ. Sci. Technol.*, 2012, **46**, 6942–6949.
15 S. Torkzaban, Y. Kim, M. Mulvihill, J. Wan and T. K. Tokunaga, *J. Contam. Hydrol.*, 2010, **118**, 208–217.
16 I. R. Quevedo, A. L. Olsson and N. Tufenkji, *Environ. Sci. Technol.*, 2013, **47**, 2212–2220.
17 B. Uyusur, C. J. Darnault, P. T. Snee, E. Koken, A. R. Jacobson and R. R. Wells, *J. Contam. Hydrol.*, 2010, **118**, 184–198.
18 C. Peyrot, C. Gagnon, F. Gagne, K. J. Willkinson, P. Turcotte and S. Sauve, *Comp. Biochem. Physiol., Part C: Toxicol. Pharmacol.*, 2009, **150**, 246–251.

19 I. R. Quevedo and N. Tufenkji, *Environ. Sci. Technol.*, 2012, **46**, 4449–4457.
20 Y. Wang, M. D. Becker, V. L. Colvin, L. M. Abriola and K. D. Pennell, *Environ. Sci. Technol.*, 2014, **48**, 10664–10671.
21 M. D. Celiz, L. A. Colon, D. F. Watson and D. S. Aga, *Environ. Sci. Technol.*, 2011, **45**, 2917–2924.
22 S. Torkzaban, S. A. Bradford, J. Wan, T. Tokunaga and A. Masoudih, *Environ. Sci. Technol.*, 2013, **47**, 11528–11536.
23 Y. Wang, H. Zhu, M. D. Becker, J. Englehart, L. M. Abriola, V. L. Colvin and K. D. Pennell, *J. Nanopart. Res.*, 2013, **15**, 1805–1821.
24 D. Kasel, S. A. Bradford, J. Simunek, M. Heggen, H. Vereecken and E. Klumpp, *Water Res.*, 2013, **47**, 933–944.
25 Y. Wang, Y. Li, J. Costanza, L. M. Abriola and K. D. Pennell, *Environ. Sci. Technol.*, 2012, **46**, 11761–11769.
26 S. Torkzaban, J. Wan, T. K. Tokunaga and S. A. Bradford, *J. Contam. Hydrol.*, 2012, **136–137**, 86–95.
27 I. Chowdhury, D. M. Cwiertny and S. L. Walker, *Environ. Sci. Technol.*, 2012, **46**, 6968–6976.
28 S. Lin, Y. Cheng, J. Liu and M. R. Wiesner, *Langmuir*, 2012, **28**, 4178–4186.
29 J. Wan, G. Zeng, D. Huang, L. Hu, P. Xu, C. Huang, R. Deng, W. Xue, C. Lai, C. Zhou, K. Zheng, X. Ren and X. Gong, *J. Hazard. Mater.*, 2018, **343**, 332–339.
30 X. Ren, G. Zeng, L. Tang, J. Wang, J. Wan, Y. Liu, J. Yu, H. Yi, S. Ye and R. Deng, *Sci. Total Environ.*, 2018, **610–611**, 1154–1163.
31 H. Dong and I. M. Lo, *Water Res.*, 2013, **47**, 419–427.
32 D. P. Stankus, S. E. Lohse, J. E. Hutchison and J. A. Nason, *Environ. Sci. Technol.*, 2011, **45**, 3238–3244.
33 Y. Wu and T. Cheng, *Sci. Total Environ.*, 2016, **541**, 579–589.
34 R. Zhang, H. Zhang, C. Tu, X. Hu, L. Li, Y. Luo and P. Christie, *J. Nanopart. Res.*, 2015, **17**, 165–176.
35 X. Jiang, M. Tong, H. Kim and J. Colloid, *Interface Sci.*, 2012, **386**, 34–43.
36 K. L. Chen, M. Elimelech and J. Colloid, *Interface Sci.*, 2007, **309**, 126–134.
37 W. W. Tang, G. M. Zeng, J. L. Gong, J. Liang, P. Xu, C. Zhang and B. B. Huang, *Sci. Total Environ.*, 2014, **468–469**, 1014–1027.
38 H. Wu, L. Cui, G. Zeng, L. Jie, C. Jin, J. Xu, J. Dai, X. Li, J. Liu and C. Ming, *Crit. Rev. Biotechnol.*, 2017, **37**, 754.
39 M. Chen, P. Xu, G. Zeng, C. Yang, D. Huang and J. Zhang, *Biotechnol. Adv.*, 2015, **33**, 745–755.
40 M. Ateia, O. G. Apul, Y. Shimizu, A. Muflihah, C. Yoshimura and T. Karanfil, *Environ. Sci. Technol.*, 2017, **51**, 7101–7110.
41 A. Amirbahman and T. M. Oison, *Environ. Sci. Technol.*, 1993, **27**(13), 2807–2813.
42 M. H. Shen, Y. G. Yin, A. Booth and J. F. Liu, *Water Res.*, 2015, **71**, 11–20.
43 S. M. Louie, E. R. Spielman-Sun, M. J. Small, R. D. Tilton and G. V. Lowry, *Environ. Sci. Technol.*, 2015, **49**, 2188–2198.
44 Y. Yin, M. Shen, X. Zhou, S. Yu, J. Chao, J. Liu and G. Jiang, *Environ. Sci. Technol.*, 2014, **48**, 9366–9373.
45 D. A. Navarro, S. Banerjee, D. F. Watson and D. S. Aga, *Environ. Sci. Technol.*, 2011, **45**, 6343–6349.
46 T. Abe, S. Kobayashi and M. Kobayashi, *Colloids Surf., A*, 2011, **379**, 21–26.
47 Y. Yin, M. Shen, Z. Tan, S. Yu, J. Liu and G. Jiang, *Environ. Sci. Technol.*, 2015, **49**, 6581–6589.
48 S. M. Louie, R. D. Tilton and G. V. Lowry, *Environ. Sci. Technol.*, 2013, **47**, 4245–4254.
49 X. Yang, Y. Zhang, F. Chen and Y. Yang, *Environ. Sci. Technol.*, 2015, **49**, 13385–13393.
50 C. V. Chrysikopoulos and V. I. Syngouna, *Colloids Surf., B*, 2012, **92**, 74–83.
51 N. Tufenkjie and M. Elimelech, *Environ. Sci. Technol.*, 2004, **38**, 529–536.
52 G. Chen, X. Liu and C. Su, *Environ. Sci. Technol.*, 2012, **46**, 7142–7150.
53 A. Franchi and C. R. O'Melia, *Environ. Sci. Technol.*, 2003, **37**, 1122–1129.
54 N. P. Sotirelis and C. V. Chrysikopoulos, *Environ. Sci. Technol.*, 2015, **49**, 13413–13421.
55 M. Zhang, S. A. Bradford, J. Simunek, H. Vereecken and E. Klumpp, *Environ. Sci. Technol.*, 2016, **50**, 12713–12721.
56 J. Yang, J. L. Bitter, B. A. Smith, D. H. Fairbrother and W. P. Ball, *Environ. Sci. Technol.*, 2013, **47**, 14034–14043.
57 A. M. Vindedahl, M. S. Stemig, W. A. Arnold and R. L. Penn, *Environ. Sci. Technol.*, 2016, **50**, 1200–1208.
58 S. L. Walker, J. A. Redman and M. Elimelech, *Langmuir*, 2004, **20**, 7736–7746.
59 T. Xia, Y. Qi, J. Liu, Z. Qi, W. Chen and M. R. Wiesner, *Environ. Sci. Technol.*, 2017, **51**, 828–837.
60 L. Cai, M. Tong, X. Wang and H. Kim, *Environ. Sci. Technol.*, 2014, **48**, 7323–7332.
61 R. R. Engebretson and R. V. Wandruszka, *Environ. Sci. Technol.*, 1998, **32**, 488–493.
62 L. L. Wang, Y. P. Chin and S. J. Traina, *Geochim. Cosmochim. Acta*, 1997, **61**, 5313–5324.
63 R. Fabris, C. W. Chow, M. Drikas and B. Eikebrokk, *Water Res.*, 2008, **42**, 4188–4196.